1   **The impact of runoff decrease and shoreline change on the salinity distribution in the wetlands of**

2   **Liao River Estuary, China**

3   Mingliang Zhang[12], Tianping Xu[1, 3], Hengzhi Jiang[4]*

4   1. School of Marine Science and Environment, Dalian Ocean University, Dalian, China;

5   2. State Key Laboratory of Coastal and Offshore Engineering, Dalian University of Technology, Dalian,
6   China

7   3. School of Marine Sciences, Sun Yat-sen University, Zhuahai, China

8   4. National Marine Environment Monitoring Center, Dalian, China

9   *Corresponding to: Hengzhi Jiang (jianghengzhi99@163.com)

10   **Abstract:** The wetland of Liao River Estuary (LRE) in northeast China is one of the best-preserved

11   wetlands across the globe. However, it is extremely vulnerable to hydrological changes as well as other

12   disturbances, particularly upstream river discharges and the reclamation from anthropogenic activities. In

13   this study, a 3D hydrodynamic model was used to reproduce the flow patterns of the LRE and to explore

14   the variation in salinity under different scenarios. Furthermore, the impact of river discharge and shoreline

15   changes on the salinity distribution in the LRE were quantitatively analyzed and discussed through several

16   simulation experiments. The model reasonably reconstructed the spatio-temporal variability and

17   distribution of salinity in the Liao River Estuary and the wetlands across intertidal areas. Increases in runoff

18   were demonstrated to significantly decrease the mean salinity values of the estuary, with changes in salinity

19   negatively correlated to the longitudinal distance from the estuary mouth. Moreover, the shoreline change

20   caused by the construction of Panjin Port was observed to have an obvious influence on the salinity

21   distribution of the LRE, particularly in the lower reaches of the Pink Beach Wetland. Comparisons of the

22   Liao River Estuary residual flow fields under different shorelines revealed that the establishment of the port

23   resulted in the diffusion of the runoff from the Daliao River due to the obstruction of the port body, which

1   enhanced the tidal mixing effect and consequently weakened the dilution effect of fresh water entering the

2   Pink Beach Wetland. Overall, the current study should be helpful for offering a greater understanding of

3   *Suaeda heteroptera* vegetation degradation in the LRE, China, and also provides a new perspective in

4   investigating the degradation mechanism in other estuarine wetlands.

5   **Keywords**: Numerical simulation, salinity distribution; coastline change, Liao River Estuary, coastal

6   wetlands

7   **1. Introduction**

8   Estuaries are located at the interface area of rivers, land and the ocean, and are commonly described as

9   enclosed or semi-enclosed bodies of water, where sea water is significantly diluted by the inflow of

10   freshwater from upstream rivers. Accumulated freshwater can potentially regulate water and salinity at

11   different temporal scales, and can offer the possibility to optimize suitable salinity conditions for animal

12   and plant habitats within the estuarine zone. Estuaries are thus considered as highly productive ecosystems.

13   As an essential component of estuaries, estuarine wetlands function as the bond connecting terrestrial and

14   coastal water ecosystems, possessing features from both terrestrial and aquatic environments. Wetlands in

15   estuaries are characterized by high biodiversity and hold the unique role of maintaining the ecological

16   equilibrium (McClain et al., 2003). Estuarine wetlands can provide substantial ecological services,

17   including flood control, sediment retention, the uptake of pollutants, carbon fixation and also act as habitats

18   for fish, waterfowl and other biotic communities (Tsihrintzis et al., 1998; Weilhoefer, 2011; Yang et al.,

19   2018).

20   Estuaries form an environment with sinuous coastlines, where rivers, streams, or creek inlets meet the

21   sea or ocean. The hydrological properties of estuaries create a complex physical environment due to the

22   combined effects of upstream rivers and the adjacent ocean. Estuary circulations are primarily controlled by

1   freshwater discharge, the tidal range and tidal currents (Sassi & Hoitink, 2013; Veerapaga et al., 2019), and

2   are modified by winds, shorelines and topography (Alebregtse et al., 2016; Lai et al., 2018), which further

3   influence the processes of salinity transport and salt-wedge in estuary waters (Haralambidou et al., 2010;

4   Gong & Shen, 2011; Liu et al., 2019). Salinity changes in estuaries have been the focal point of much work

5   over the past few decades in order to understand saltwater intrusion mechanisms, with the majority of the

6   research based on on-site observations and numerical models. Early studies analyzed observation data to

7   investigate the salt intrusion phenomenon in estuaries, with further evaluations performed on estuary

8   mixing type, salt intrusion distance, salinity distribution and the current circulation (Pichard 1952, 1954;

9   Hansen & Rattray, 1965). This was followed by field surveys via instrumentation of Acoustic-Doppler-

10   Current-Profilers (ADCP) and Conductivity-Temperature-Depth (CTD), whereby researchers investigated

11   the salinity distribution characteristics and the salt transport mechanisms in the Hudson River estuary

12   (Bowen & Geyer, 2003; Lerczak & Geyer, 2006). Studies suggested that the salt intrusion in an estuary is

13   maintained by two opposite longitudinal transport processes: i) An advection resulting from fresh water

14   outflow, which tends to drive salt out of the estuary; and ii) a down gradient advection, which drives salt

15   landward (Lerczak & Geyer, 2006). The salinity patterns in estuaries were also demonstrated to be the

16   result of additional factors, such as the longitudinal advection and vertical mixing (MacCready, 2010;

17   Scully & Geyer, 2012).

18   The development and application of numerical models have been a key component of research on the

19   salt transport and saltwater intrusion in estuarine waters at high spatial and temporal resolutions. For

20   example, Zhao et al. (2010) simulated wetland-estuarine-shelf interaction processes at the Plum Island

21   Sound and Merrimack River system in the Massachusetts coast using the three-dimensional (3D)

22   unstructured-grid, finite volume coastal ocean model (FVCOM), where the water exchange was observed

to vary with the magnitude of freshwater discharge and wind conditions. Gong (2011, 2018) employed the Environmental Fluid Dynamics Code (EFDC) and the Coupled-Ocean-Atmosphere-Wave-Sediment Transport (COAWST) to investigate the effects of local and remote winds and wind waves on salt intrusion in the Modaomen and Pearl River estuaries, respectively, with conclusions having an applicability to other partially mixed estuaries under the threat of salt intrusion. Popescu et al. (2015) presented a 3D hydrodynamic model to understand the hydrodynamics of the Danube Delta wetlands, demonstrating the strong impact of the Danube River variable discharges on the habitats and the overall ecological status of the delta. Andrews et al (2017) applied the 3D hydrodynamic model to examine the impacts of anthropogenic changes (land use changes, levee construction, channel modifications etc.) on the physical characteristics and salt intrusion processes at the San Francisco Estuary. Wang et al (2019) combined the FVCOM model with long-term field survey data to investigate the seasonal variability of currents and salinity in the Indus River Estuary. Results revealed that the salinity intrusion distance was principally controlled by river discharge in the estuary, while the seawater intrusion was significantly impacted by tidal forcing in the absence of river runoff. Tian (2019) combined field data collected in the Chester River Estuary with FVCOM to identify the driving factors and their relative importance in controlling the saltwater intrusion variability across time. Results demonstrated that river discharge was the primary factor controlling saltwater intrusion changes over inter-annual time scales, while sea surface levels dominated the seasonal variations (Tian, 2019). Estuarine salinity has a significant effect on the growth of coastal wetland plants and plays an important role in maintaining the ecological health of estuarine wetlands (Song et al. 2009). Despite this, studies on the spatial and temporal distribution of salinity in estuarine wetlands are limited, with most work generally focusing on salinity transport and saltwater intrusion mechanisms along the estuaries (Ralston et al., 2008; Haralambidou et al., 2010; Veerapaga et al, 2019; Wang et al., 2019).

The Liao River in northeastern China is one of the seven largest rivers in the country and ends at the LRE located at the top of Liaodong Bay (Fig. 1a). Due to the recent rapid urban sprawl and growth in population, water consumption has increased dramatically in the Liao River basin. In addition, the upstream closure projects have directly led to a sharp decrease of the downstream runoff of Liao River into the Liaodong Bay, which may further affect the exchange and mixing of salt water and fresh water in the estuary (Ralston et al, 2008; Gong et al, 2011). Panjin Port is located on the southeast of the LRE, adjacent to the Daliao River (Fig. 1b). The port was founded in 1995, completed in 1999, and following more than 10 years of continuous expansion, the existing land area has reached 230,000 m^2. The construction of Panjin Port is of great importance for the development of the local economy, yet its construction has also been problematic. The large area of marine reclamation has resulted in drastic changes in the southeast coast of the LRE since 1995 (Fig. 1b and c). Large areas of marine reclamation can alter both the local topography and the original coastline (Jia et al., 2018). Changes in the shoreline will have an impact on the characteristics of the original flow field, which can consequently affect the transport processes of ocean materials, including sediment transport, pollutant diffusion and salinity distribution (Alebregtse et al., 2016).

Suaeda heteroptera is one of the most common pioneer salt-tolerant plants in the LRE. Large area of *Suaeda heteroptera* community grows in intertidal zone along the east coastline of the LRE, forming a unique natural landscape which is known as the Pink Beach Wetland. According to satellite images and on-site observations, the wetlands in the LRE have experienced severe degradation over the past decade, particularly in the Pink Beach Wetland (PBW) close to the northwest of Panjin Port (Wang et al., 2020). Much effort has been made to investigate the growth mechanisms and influencing factors of vegetation *Suaeda heteroptera* in salt marshes (Song et al., 2009; Wang et al., 2010; Sun et al., 2016). Experiments

Landsat image of intermediate and eastern area of the LRE in 2019 (from Geospatial Data Cloud http://www.gscloud.cn/sources/). The black elliptical shape represents the PBW region, and the black rectangular denotes the Panjin Port area. **(c)** The Landsat image of eastern LRE in 1995. **(d)** The bathymetry of the LRE waters (positive values represent water depth and negative values indicate land elevation), the observation stations and analysis gauges. The blue triangles denote the tidal stations, the red circles are the tidal flow and salinity observation stations, while the black circles represent the analysis gauges used for salinity comparison.

In this study, the FVCOM system was combined with field observations to investigate the effect of anthropogenic shoreline changes on the salinity distribution in the LRE. The principle aims of this study are to: (1) evaluate and quantify the effect of shoreline changes resulting from the port construction on estuary circulations and salinity distributions in the LRE; (2) explore the potential influence of these variations on growth of *Suaeda heteroptera* in tidal wetlands in the LRE; and (3) provide a reference for wetland conservation and water resource utilization in the LRE. The rest of the paper is organized as follows. A brief introduction of the study area is described in Section 2. Section 3 provides a description of the FVCOM model and demonstrates the implementation of the modeling system and model validation, including tidal level, flow and salinity. The effects of shoreline change resulting from port construction on residual flow and the spatial-temporal distribution of salinity in the LRE are analyzed and discussed in detail in Section 4. Finally, the general conclusion of the manuscript is detailed in Section 5.

2. Study area

The LRE, situated in the northwest of Liaoning Province, China, is a funnel-shaped shallow estuary that exhibits a decrease in width from 20 km at the mouth to 1 km at the upstream reach. It is a momentous ecological economic zone in the north of the Liaodong Bay, playing an important role in the comprehensive

development of the marine industry and fishing economy in northeastern China. The bathymetry of the

LRE is complicated, with the formation of many shallow shoals due to sediment deposition. The water

depth ranges from < 3 m in the shoals to < 7 m in the main channels. The tidal feature in Liaodong Bay

fundamentally belongs to semidiurnal tide, in addition, except the region along the coast of Liaoning

Province in which semidiurnal tide predominates, most marine domains are under the control of diurnal

tide (Liu et al., 2005). The upstream river network of the LRE is relatively simple, mainly dominated by the

Liao River and is also affected by the river discharge from the Daliao River. The multi-year average river

discharge of the Liao River ranges from 101 m^3/s in the dry season to 285 m^3/s in wet season (Qiao et al.,

2018), barely reaching 450 m^3/s under extreme precipitation conditions.

3. Methods

3.1 Model description

The FVCOM was adopted to simulate tidal flow and salinity in the LRE. It is a three-dimensional ocean

model which was originally developed by Chen et al. (2003) and improved by researchers at the University

of Massachusetts-Dartmouth (UMASSD) and Woods Hole Oceanographic Institution (WHOI) (Chen et al.,

2006). Previous applications include research on large lakes, coastal estuarine regions, and regional ocean

areas (Gronewold et al., 2019; Lin & Fissel, 2014; Lai et al., 2018). The modelling system uses an

unstructured triangular grid that can accurately fit complex shorelines, which is helpful for small-scale

simulations (such as estuarine wetlands) with high resolution. FVCOM is originally coded for sigma-

coordinates in the vertical direction (Chen et al., 2006), the application of terrain-following coordinates

results in an improved capacity to solve complex bathymetric conditions (Haney, 1990). In addition, the

ocean circulation model employs the modified level 2.5 Mellor and Yamada and Smagorinsky turbulent

closure schemes for vertical and horizontal mixing.

3.2 Model configuration

The model domain covers the whole sea region located at the top of the Liaodong Bay, including the Liao River and the Daliao River, extending from the 40.303 ° to 40.710 ° northern latitudes and the 121.029 ° to 122.031 ° eastern longitudes. In order to visually reflect the shoreline changes resulting from the construction of Panjin port, two coastlines of the port area were manually extracted from Landsat image collected in 1995 and 2019 (from Geospatial Data Cloud http://www.gscloud.cn/sources/?cdataid=263&pdataid=10) using ArcGIS software. The remaining coastline of the LRE was manually extracted from Google Earth software (with higher spatial resolution). As shoreline changes in other area of the LRE were relatively less significant over the time span, two port coastlines were then respectively reconnected with the same remaining coastline in the finite-element Surface-water Modeling System by Acquaveo (Chen et al., 2006), which was applied to generate an unstructured triangular mesh for the LRE domain. The bathymetry of the computation domain was derived from the Navigation Guarantee Department of the Chinese Navy Headquarters (China Navigation Publications Press) and the topographic survey data in the upstream of the LRE measured by us. The total number of grid nodes and elements were 9501 and 17938 for grid 1995 (Fig. 2b), and 13699 and 25928 for grid 2019, respectively (Fig. 2c). The largest lateral and longitudinal lengths of the model domain were 113 km and 67 km, respectively, while the spatial resolution of the model grids varied from 2500 m at the external open boundary to 60 m at the intertidal area of the wetland domain.

The three-dimensional baroclinic mode with 11 vertical sigma levels was adopted for the modelling system, with the external and internal mode time steps set to 2 s and 10 s, respectively. The model was driven by water level derived from the Bohai Sea tidal model using the MIKE 21 hydrodynamic model Model at the open boundary. The initial condition for velocity is zero everyhere. The open boundary

1 condition for salinity was set to 34 PSU at the sea surface and interpolated between 34 and 32 PSU along

2 the sigma layers, and that for temperature was set to uniform 15 ℃ from the surface to the bottom. The

3 initial condition for salinity was based on the quasi-steady result derived by running the model for

4 approximately four months. Considering that the average water depth of the LRE is relatively small,

5 variation of temperature in horizontal and vertical directions is negligible, the initial temperature field was

6 set to a uniform value 15 ℃ across the whole domain accordingly. Furthermore, four case studies were set

7 up based on two computational grids and two different river discharge conditions, as illustrated in Table 1.

8 Following this, the river discharges of the Liao River and Daliao River were set to 25 m^3/s and 48m^3/s (285

9 m^3/s and 266 m^3/s), indicating a decreased runoff circumstance during the dry season (annual average

10 runoff), respectively (Qiao et al, 2018).
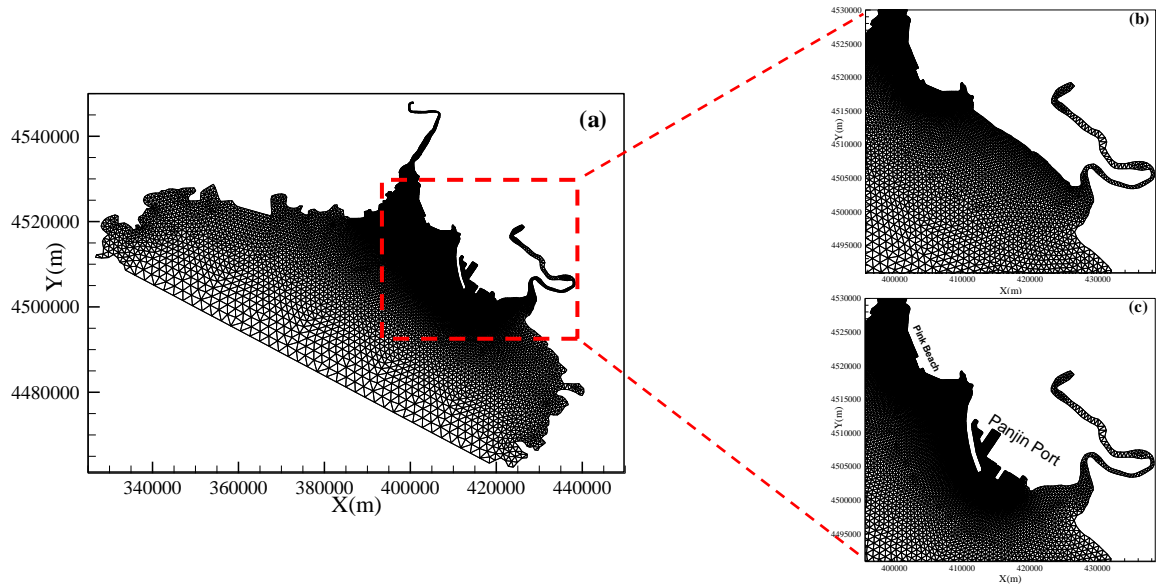
12 **Figure 2.** Mesh sketch of the LRE **(a)** and detailed meshes for the Panjin Port region in 1995 **(b)** and 2019

13 (c).

14 **Table 1.** Model case study settings.

Case Study	Grid	River Discharge(m³/s)	
		Liao River	Daliao River
Case1	2019	25	48
Case2	2019	285	266
Case3	1995	25	48
Case4	1995	285	266

3.3 Model validation

To validate the model's performance in the simulation of the tidal dynamics and salt transport in LRE, the simulated results were compared with the available measured data. Thereinto, two tide level stations (T1 and T2), four tidal flow observation stations (V1, V2, V3 and V4), two salinity measuring gauges (V1 and V2) and four wetland salinity analysis sites (S1, S2, S3 and S4) were selected to evaluate and analyze the model performance in the study domain. Table. 2 gives the specific coordinate information about the eight stations. The model simulations cover the period from 20 April to 10 September 2018. The tide level was verified from 0:00 on 1st May to 23:00 on 31 May 2018. The periods of tidal flow validation were divided into neap tide and spring tide, of which the neap tide period was from 11:00 on 8 June to 10:00 on 9 June, 2018, and the spring tide period from 6:00 on 15 June to 5:00 on 16 June, 2018. The salinity data was measured at V1 and V2, with a validation period from 5:00 on 10 September to 4:00 on 11 September 2018 for V1, and from 6:00 on 10 September to 5:00 on 11 September 2018 for V2.

The comparison between modelled and observed data was quantified using the root mean square error (RMSE) and the predictive skill score (Skill). The magnitude of the RMSE indicates the average deviation between the simulated results and the observed data, while the predictive skill score represents the degree to which the simulated value fits the measured value (1 = perfect fit, 0 = complete difference). The RMSE and Skill are defined as follows:

$$\text{RMSE} = \sqrt{\frac{\sum_{i=1}^{n}(M_i - O_i)^2}{n}} \tag{1}$$

$$\text{Skill} = 1 - \frac{\sum_{i=1}^{n}(M_i - O_i)^2}{\sum_{i=1}^{n}(|M_i - \bar{O}| + |O_i - \bar{O}|)^2} \tag{2}$$

where M_i and O_i represent the modeled results and observed values, respectively, $\bar{O}$ indicates the mean of the observed values, and n is the number of observed data points.

Table 2. Coordinate information of gauging stations

Stations	Longitute (°E)	Latitude (°N)
T1	122.150	40.364
T2	121.065	40.790
V1	121.913	40.739
V2	121.744	40.790
V3	121.849	40.796
V4	121.776	40.836
S1	121.839	40.840
S2	121.892	40.804
S3	121.924	40.805
S4	121.767	40.886

2 Figure 3 presents the tide level comparison results. The simulated water levels at T1 and T2 are

3 observed to agree well with the measured data. In general, the amplitudes of the modeled results are

4 consistent with the observations, with a maximum phase difference of less than 30 minutes. The harmonic

5 analysis was also performed in this study, the model results are in good agreement with the observations for

6 the main component M2 in the two stations. Where the differences between the model and field data are

7 smaller than 9 percent for the amplitude and 10 degrees for the phase. Despite this, several significant

8 errors are observed between the simulated high and low tide levels and the observed values. This may be

9 attributed to the inaccurate open boundary water level conditions. The comparisons of the simulated and

10 measured flow speeds and directions during neap and spring tides are presented in Figure 4 and Figure 5,

11 respectively. In general, the modeled tidal flow exhibits a better match with the observation data in neap

12 tide compared to spring tide. The poorer spring tide fitting results may be a result of the following: (1) The

13 open boundary conditions adopted in the model may be inaccurate for certain periods; (2) the bathymetry

14 used in the model may differ to that of the study area due to recent sediment deposition; and (3) the model

15 employed a uniform bed roughness coefficient across the whole area. Figure 6 displays the comparisons of

16 simulated and observed salinity at V1 and V2. The simulated salinity is in good agreement with the

17 measured data, with broadly consistent trends in variation between datasets. Table 3 gives the results from

1   the error quantification analysis of the simulated tide level (ζ), tidal flow ($\overline{U}$) and salinity ($\bar{S}$). The Skill

2   scores for the T1 and T2 tide levels are both greater than 0.95, while flow velocities exceed 0.80. The

3   results indicate that the model established in this paper can accurately reproduce the hydrodynamic

4   processes in the LRE. The determined Skill values for salinity indicate that the model effectively

5   reproduces the salinity variations at V1, yet slightly under-estimates the salinity at V2. The high simulation

6   accuracies of the water level, currents and salinity determined by the proposed model in the study area

7   demonstrates that the model is suitable for further studies on the salinity distribution in the LRE.
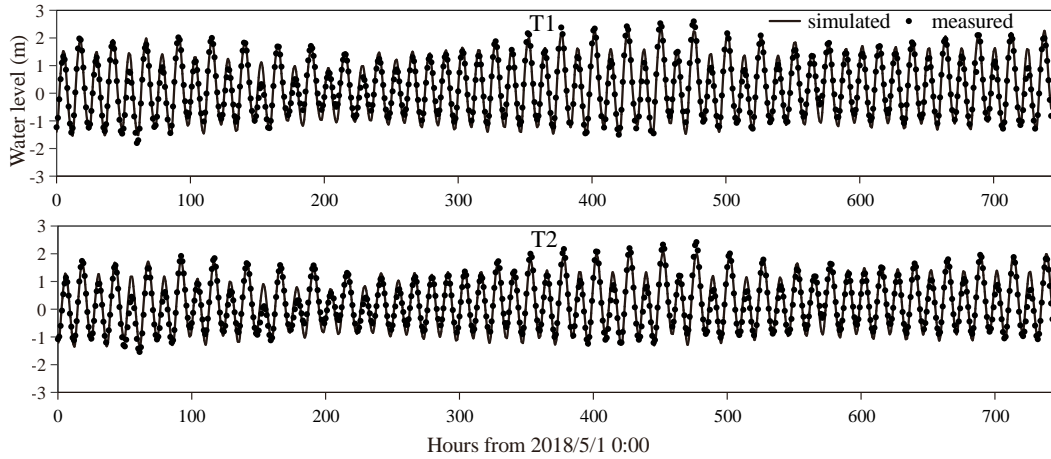
10   **Figure 3.** Comparison of the simulated and measured water levels at T1 and T2.
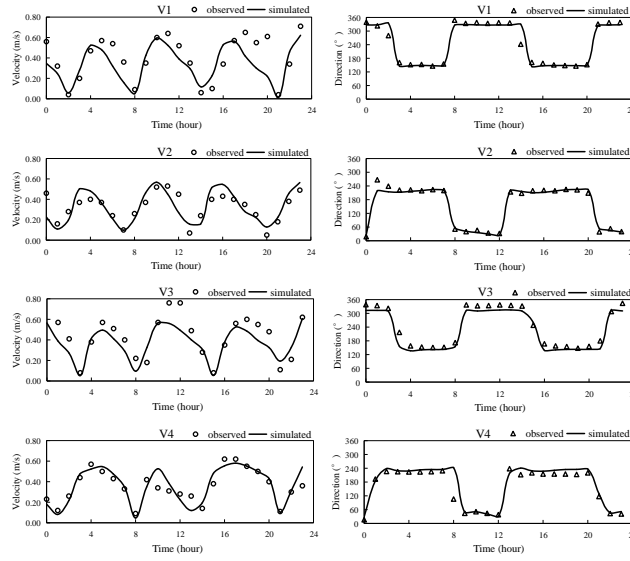
2   **Figure 4.** Comparison of simulated and measured tidal currents at the monitoring stations during neap tide.
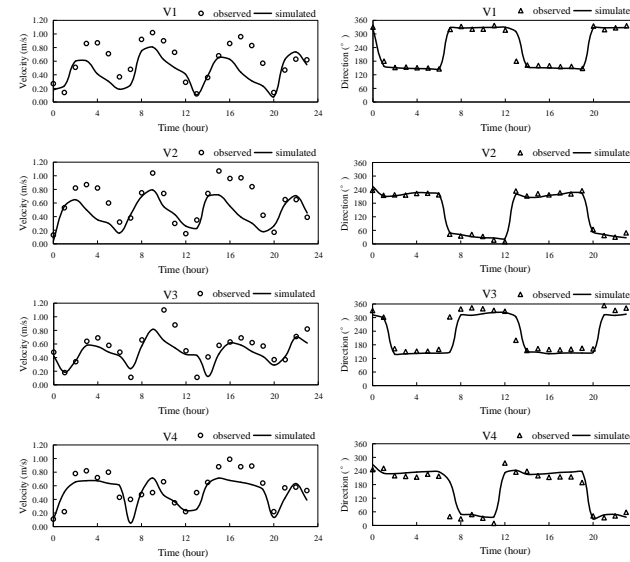
4   **Figure 5.** The comparison of simulated and measured tidal currents at the monitoring stations during spring

5   tide.
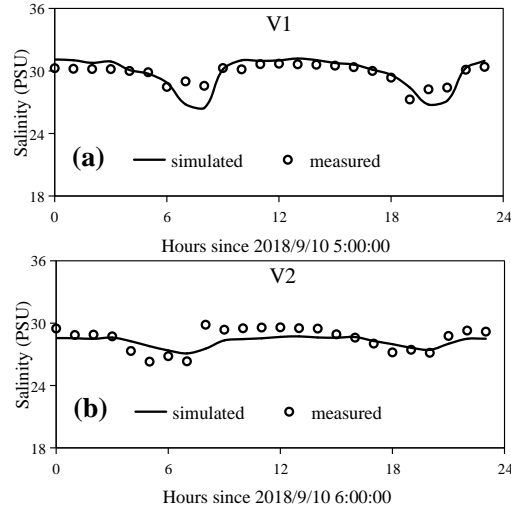
Figure 6. Validation of salinity at (a) V1 and (b) V2.

Table 3. Error analysis of simulated and measured values.

Stations	RMSE			Skill		
	ζ(m)	$\bar{U}$(m/s)	$\bar{S}$(psu)	ζ(m)	$\bar{U}$(m/s)	$\bar{S}$(psu)
T1	0.248	—	—	0.985	—	—
T2	0.305	—	—	0.969	—	—
V1	—	0.207	0.888	—	0.808	0.859
V2	—	0.196	0.877	—	0.809	0.701
V3	—	0.160	—	—	0.849	—
V4	—	0.137	—	—	0.891	—

4 Results and discussion

4.1 Effect of river discharge on salinity distribution in the LRE

To explore the effect of river discharge on salinity transport in the LRE, two experimental cases were

established (Case 1 and Case 2). An average value of 50-h was chosen to reflect the irregular semi-diurnal

tidal characteristics of the LRE. The salinity distribution characteristics at the surface and bottom layers are

generally consistent due to the shallow water depth in the LRE, salinity difference along the vertical was

inapparent, thus the vertical averaged salinity value was selected for analysis. The 50-h averaged salinity

distributions of the LRE during spring and neap tides under different runoff conditions are shown in Fig. 7

and Fig. 8. For Case 1, the salinity values in the middle of this estuary during neap and spring tides are

1   maintained between 16-28 PSU and show a low longitudinal gradient from downstream to upstream. In

2   Case 2, the salinity values of the middle LRE decease significantly and vary between 4-20 PSU, the

3   longitudinal salinity gradient becomes higher compared with Case 1. As the tidal current movement

4   strengthens during the spring tide period, the saltwater intrusion distance in the estuary consequently

5   increases compared to that during the neap tide period. To quantify the effect of river discharge on the

6   salinity of LRE, the 30-day averaged salinities of eight stations at the surface and bottom layers for Case 1

7   and Case 2 were compared in Fig. 9. The salinity of the LRE is observed to decrease dramatically as the

8   river discharge increases to mean level. As shown in Fig. 9(b), the averaged salinities of the eight sites in

9   Case 2 decreased by 84.9%, 28.8%, 14.6%, 68.1%, 16.5%, 40.0%, 46.5% and 46.1%, respectively,

10   compared with those in Case 1. As a result, the salinity of the LRE varies with runoff condition and tidal

11   strengthening. Variation in river discharge exerts a significant effect on the longitudinal distribution of

12   salinity in the estuary. Due to the construction of closure projects in the upper reaches of the Liao River, the

13   quantity of freshwater discharge from the Liao River into the Liaodong Bay has decreased sharply, which

14   directly weakening the river flow's resistance to the tides and further strengthen the salt intrusion in the

15   estuary. In addition, decrease in runoff will alter the tide duration in estuary. For vegetation in salt marshes,

16   the prolonged retention time of salt water will further increase duration of salt stress which may result in

17   negative effects on vegetation growth. Thus, as river discharge in the head of LRE sharply dropped over the

18   past decade, it is reasonable to speculate that the corresponding salinity increase and prolonged salt water

19   retention will have restrain effects on growth of *Suaeda heteroptera* in the estuarine wetlands, which could

20   potentially lead to the degradation of salt marshes and the destruction of estuary ecosystems in the LRE.
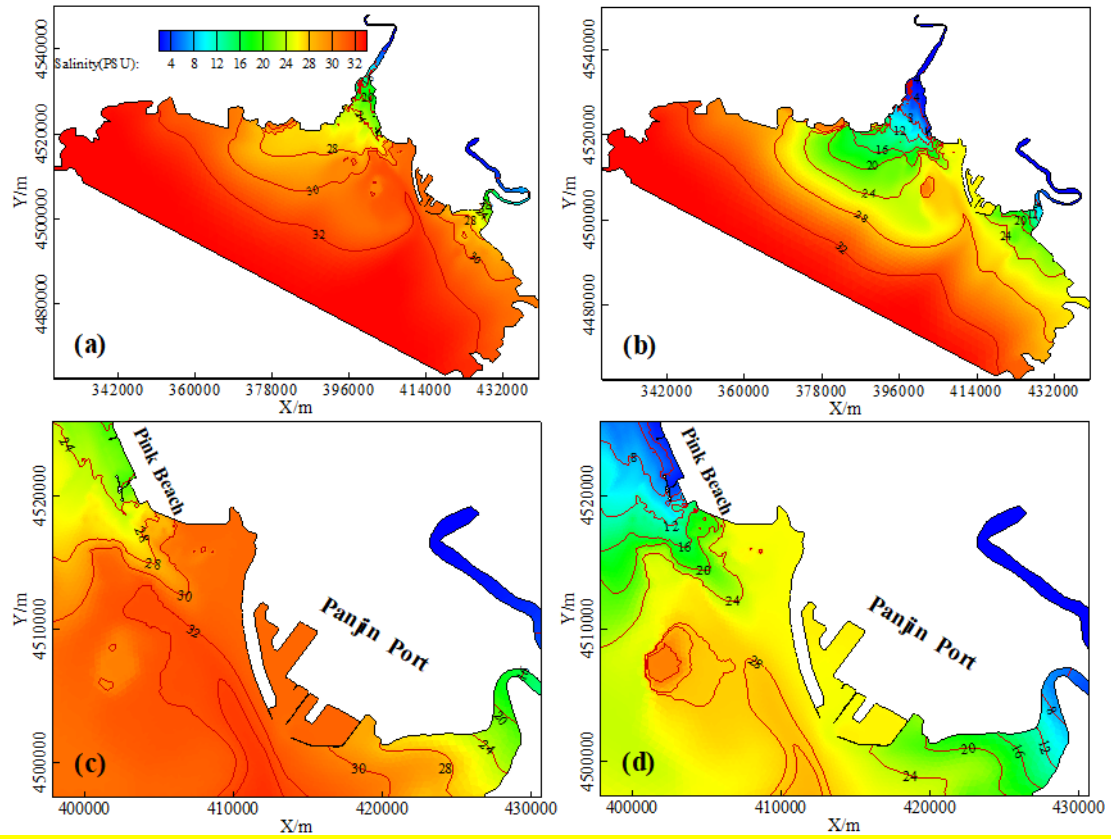
3 **Figure 7.** Simulated distribution of 50-h averaged salinity in the LRE during a spring tide for Case 1 (left

4 panel) and Case 2 (right panel).
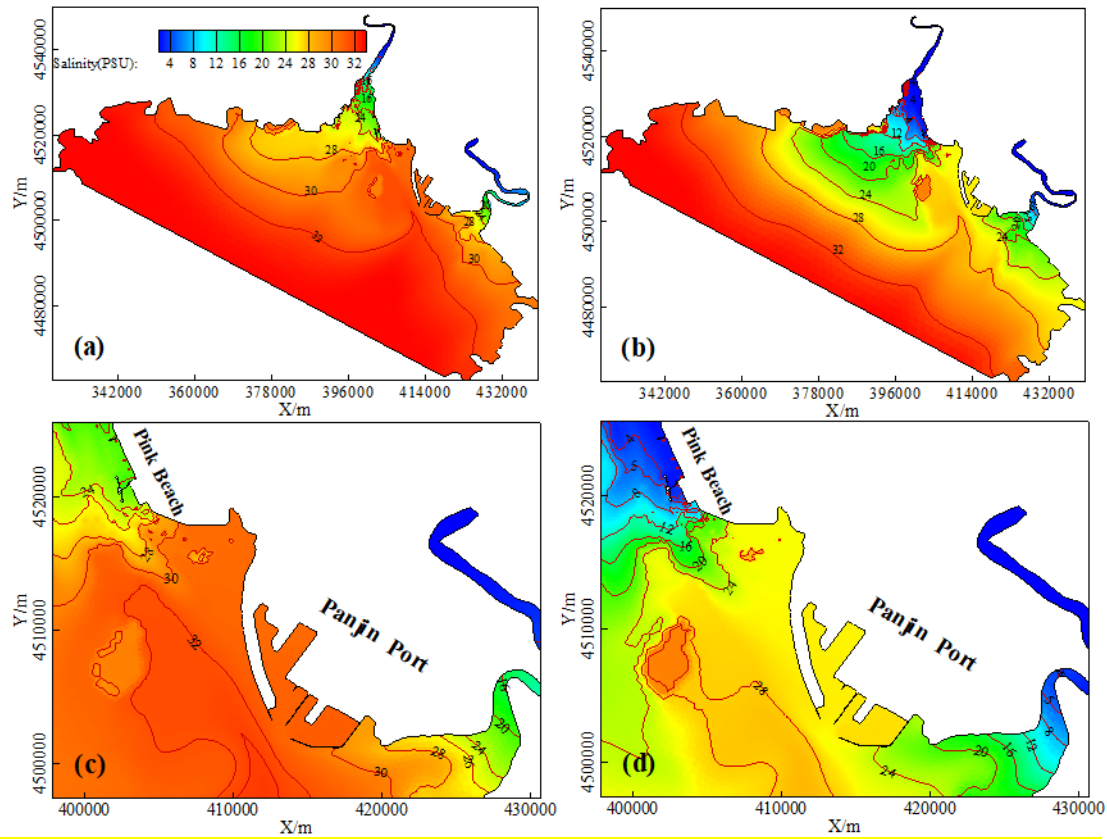
2 **Figure 8.** Simulated distribution of 50-h averaged salinity in the LRE during a neap tide. Panel (a) and

3 panel (c) for Case1; panel (b) and panel (d) for Case2.
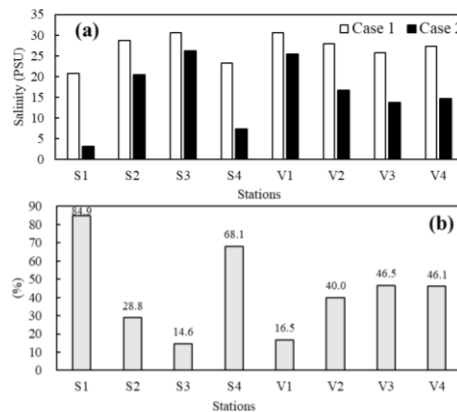
6 **Figure 9.** Panel (a) comparison of 30-day averaged salinity at the eight stations for Case 1 and Case 2;

7 Panel (b) the decrease percentage of salinity values in Panel (a).

8 **4.2 Effect of shoreline change on salinity distribution in the LRE**

9 The majority of salt marsh plants in the LRE grow on the tidal flats along the coast, and are thus submerged

10 by sea water at high tide and are exposed at low tide. This unique growth environment complicates the

11 research on the degradation mechanisms facing such vegetation. Consequently, we applied numerical

1   simulations to overcome this obstacle, focusing on the influence of shoreline change caused by

2   anthropogenic activity on the salinity distribution of LRE. In addition, we further discussed the potential

3   relationship between shore change and tidal wetland degradation in the LRE. To investigate the influence of

4   shoreline change caused by the port construction on the salinity distribution in the LRE, the computational

5   grids generated by two shorelines in 1995 (pre-port construction) and 2019 (post-port construction) were

6   adopted for salinity simulations in the LRE. The simulated results of the two grids were then compared and

7   analyzed. Figures 10 and 11 show the average salinity distribution calculated by grid 1995 during a spring

8   tide and a neap tide under different runoff conditions, respectively. In general, the salinity of the LRE in

9   1995 exhibits a significant decrease under high river discharge, with the longitudinal salinity gradient

10   becoming more pronounced. It can be seen from Fig. 8 (9) and Fig. 10 (11) that salinity distribution during

11   spring tide (neap tide) in 1995 evidently differ from that in 2019, especially at the east LRE where the

12   Panjin Port built. For a more intuitive comparison, the isohalines of the LRE under a low and a high runoff

13   conditions were plotted using the results from the two grids, as shown in Fig. 12. The green isohalines (grid

14   2019) are located upper the red isohalines (grid 1995) in the estuary waters during both runoff conditions,

15   particularly in the eastern region of downstream PBW. This indicates the intensification of the shoreline

16   change with the intrusion of salt water.
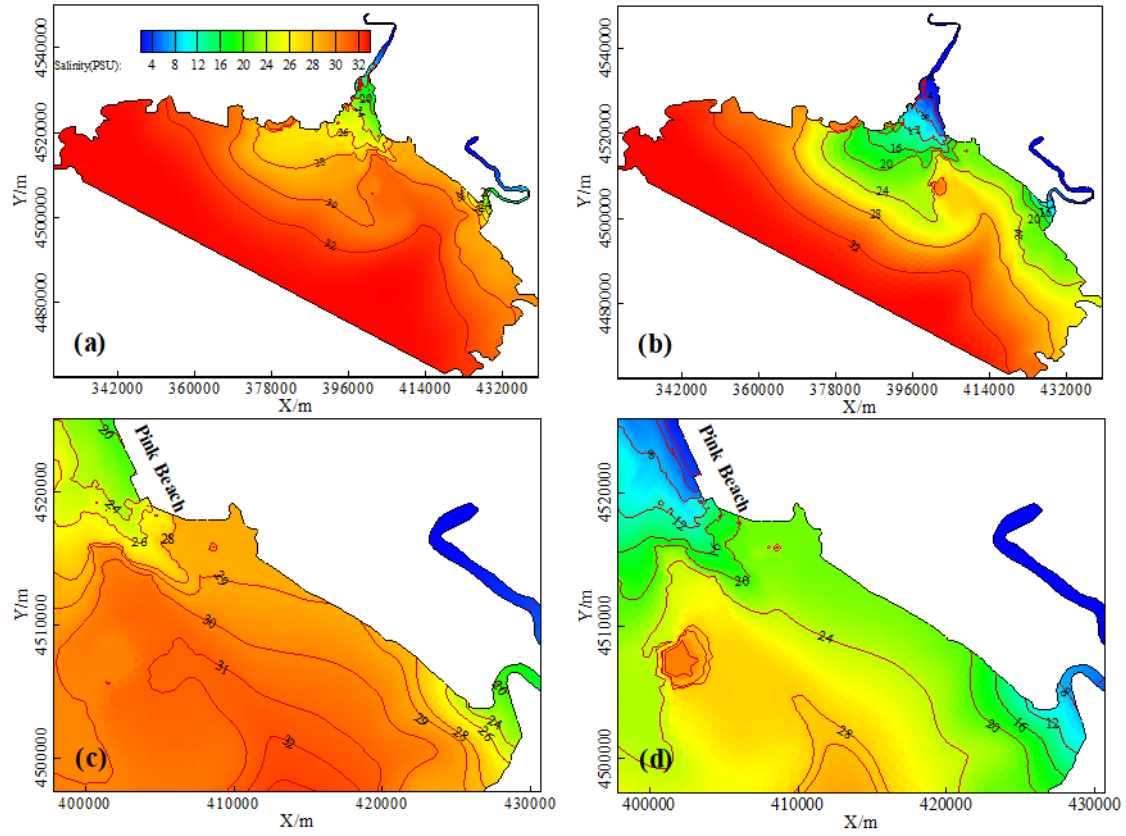
Figure 10. Simulated distribution of 50-h averaged salinity in the LRE during a spring tide. Panel (a) and panel (c) for Case3; panel (b) and panel (d) for Case4.
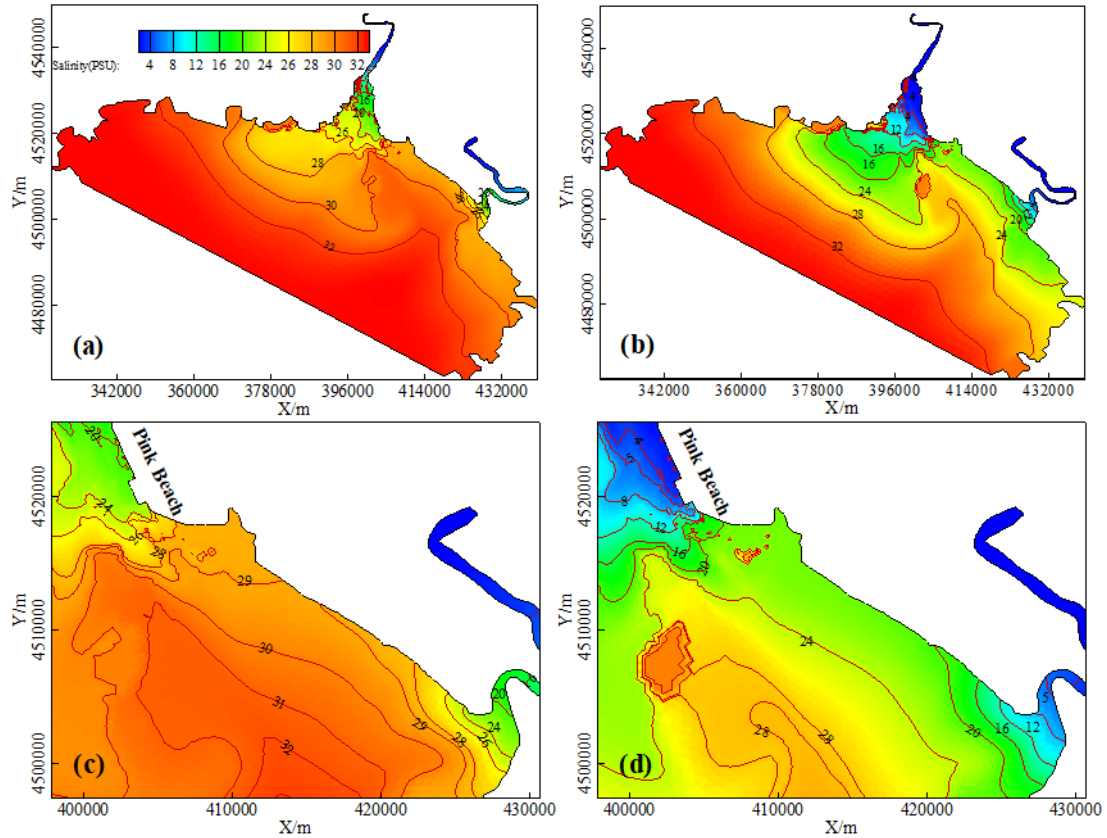
Figure 11. Simulated distribution of 50-h averaged salinity in the LRE during a neap tide. Panel (a) and panel (c) for Case3; panel (b) and panel (d) for Case4.
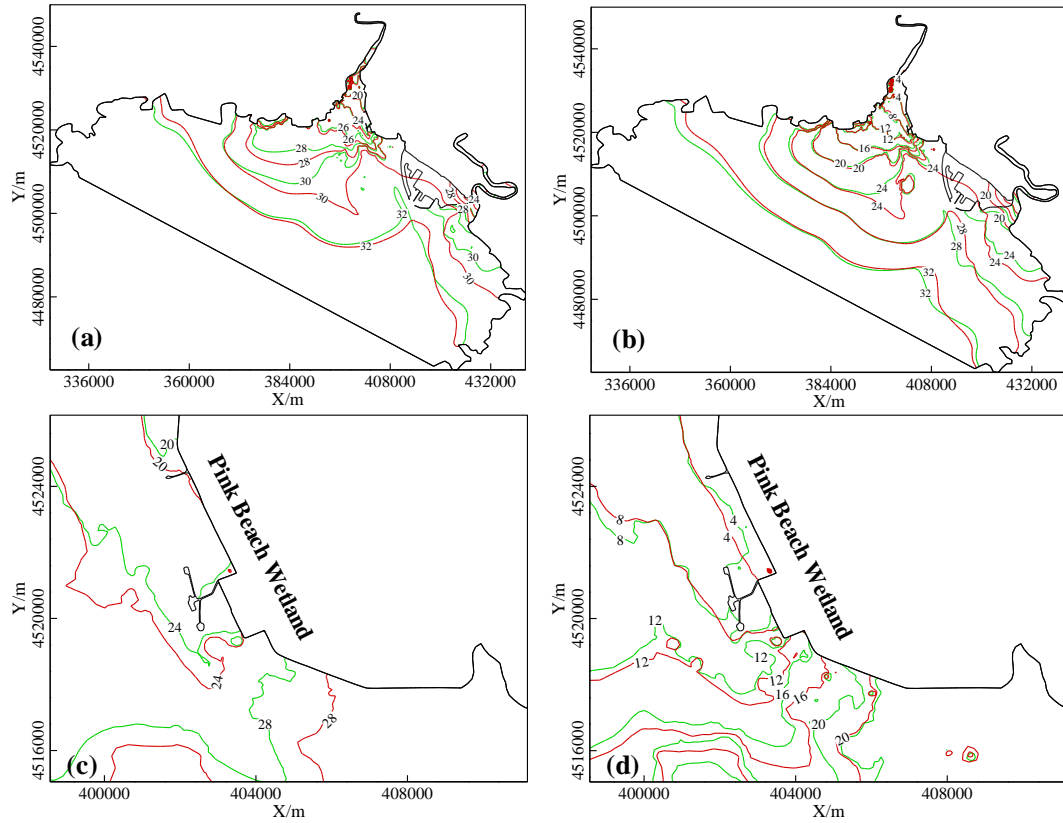
2 **Figure 12.** Comparison of 50-h averaged isohalines simulated by grid 2019 (green solid line) and grid 1995

3 (red solid line) in low runoff condition (left panel) and mean runoff condition (right panel).

4   To quantify the influence of shoreline changes on the salinity of the LRE, we compared the 30-day

5 averaged salinities determined via the two grids at the eight monitoring sites as shown in Fig. 13. For Case1

6 and Case3 (low runoff condition), following the construction of the Panjin Port, the averaged salinities of

7 the eight stations (S1, S2, S3, S4, V1, V2, V3 and V4) increased by 4.4%, 6.2%, 7.9%, 0.7%, 4.5%, 2.6%,

8 5.1%, 2.6%, 5.1% and 2.3%, respectively, and that for Case 2 and Case 4 (mean runoff condition) increased

9 by -0.6%, 14.5%, 20.9%, -1.3%, 6.9%, 2.2%, 11.0% and 1.4%, respectively. These results indicate that the

10 shoreline change caused by the extensive sea reclamation for the construction of Panjin Port has a

11 considerable effect on the salinity distribution in the LRE, particularly in the downstream PBW (S2, S3) on

12 northwest Panjin Port. This increase is observed to be greater under mean runoff condition compared to low

13 runoff condition, with a maximum increase in salinity over 4 PSU.
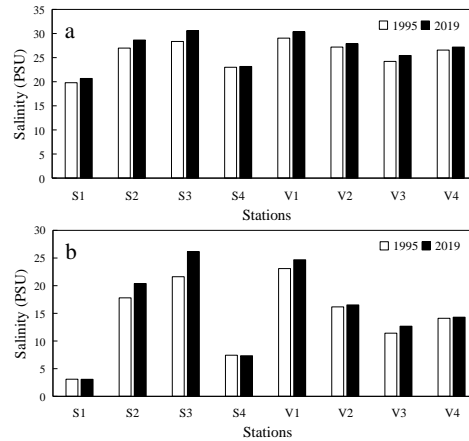
Figure 13. 30-day averaged salinities of the eight monitoring stations derived from the grid 1995 and grid

2019 in (a) low runoff condition; (b) mean runoff condition.

4.3 Effect of shoreline change on flow patterns in the LRE

To investigate the relationship between the flow field and salinity variation as a function of shoreline

changes due to reclamation, we analyzed the residual flow fields of the LRE with and without the Panjin

Port. The results were then used to illustrate the underlying mechanism leading to variation in salinity in

terms of fresh water transport. Comparisons of the residual flow fields of the LRE under the two shoreline

conditions (Fig. 14) demonstrate that at the 1995 shoreline, a residual flow induced by the runoff from the

Daliao River traveled along the coastline to the downstream of the PBW, diluting the sea water due to the

constant replenishment of fresh water. Following the port establishment, the residual current to the south of

the port exhibited significant changes in both its magnitude and direction, with an eastward flow that

subsequently moved southeastwards. A residual was observed around the tip of the LRE with a strong

(approximately 20 cm/s) clockwise circulation close to the Panjin Port, resulting from a flood-dominant

north and ebb-dominant south shore. The spatial distribution of the residual currents exhibited a similar

trend during both neap and spring tides. The obstruction of the port body and enhanced tidal mixing effect

resulted in the diffusion of the Daliao River runoff, weakening the fresh water dilution effect on the

seawater. This can explain the higher salinity in the PBW following the shoreline changes in 2019. In

1 summary, with the decrease of the upstream river discharge, the construction of Panjin Port has had a

2 marked effect on the variation of salinity in the LRE, with impacts including the potential degradation of

3 wetlands, particularly the Pink Beach Wetland.
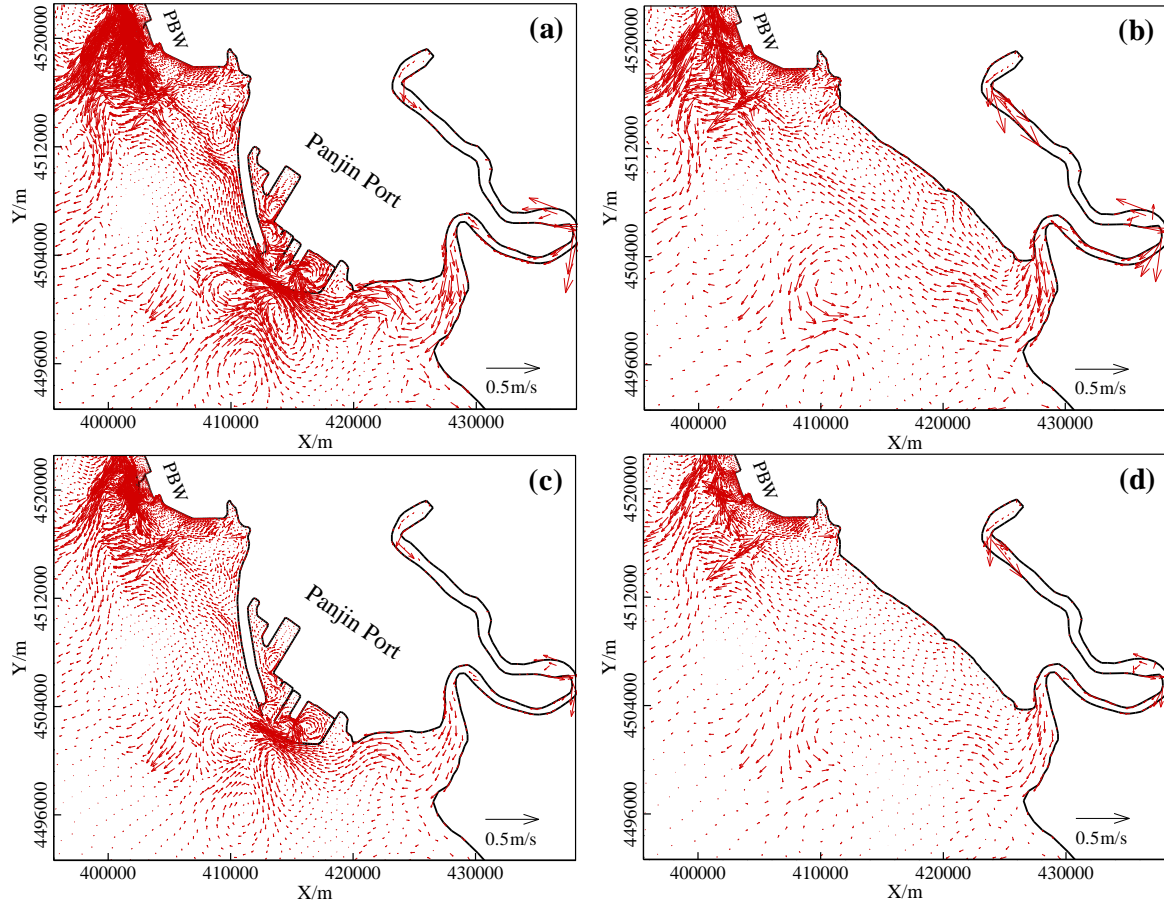
5 **Figure 14.** Residual flow at the (a)-(b) surface layer and (c)-(d) bottom layer for grid 2019 (left panel) and

6 grid 1995 (right panel).

7 **5 Conclusions**

8   In this paper, a three-dimensional numerical model was applied to investigate the influences of river

9 discharge and shoreline changes on the salinity distribution in the LRE. Two runoff conditions were set to

10 represent different water seasons in the estuary. Data derived from Landsat satellite imagery and adapted

11 using Google Earth software was employed to extract the LRE shorelines in 1995 and 2019. These were

12 then used to generate the computational grids for tidal current and salinity distribution simulations of the

LRE before and after the construction of Panjin Port. Simulation results indicate that the variation of river discharge has a significant effect on the longitudinal distribution of salinity in the LRE. Runoff increases can significantly decrease salinity in estuary waters due to the dilution of freshwater. Furthermore, the changes in shoreline triggered by the construction of Panjin Port has noticeable effect on the salinity transport in the LRE, with the Pink Beach Wetland in northwest Panjin Port observed to be the most effected. There is a rise in the water salinity amongst the wetlands located within the lower reaches of the Pink Beach Wetland following the construction of the port. The rate of increase is greater during the wet season compared to the dry season, with a maximum increase in salinity of 4 PSU. Comparing the residual flow field simulated using the two shoreline conditions reveals that prior to the port construction, the runoff-induced residual flow from the Daliao River travelled along the shoreline to the lower reaches of the Pink Beach Wetland, where it then accumulated. This continuous supply of fresh water diluted the sea water and reduced the salinity. Once the port was constructed, its obstruction of the port area strengthened the tidal current mixing, and the partial runoff from the Daliao River was diverted. As a result, the fresh water dilution effect further weakened, thus increasing the salinity of the sea water in the lower reaches of the Pink Beach Wetland.

The ecological degradation of partly wetlands in the LRE has become more and more severe in the past decade, especially in the southern seas. This is attributed to long-term disturbances resulting from anthropogenic activity, including river closure projects, agriculture irrigation, and coastal constructions. Despite this, key physical processes in the LRE have yet to be systematically investigated and understood in terms of river discharge, wind, wave and complex terrain conditions. The influences of wind stress, estuary topography variations and water resource utilization in upper rivers on the spatial-temporal distribution of salinity in the LRE will be the focus of future work.

1 **Author contributions.**

2 All authors contributed to the design and development of the work. The experiments were originally carried

3 out by MZ and TX. HJ carried out the data analysis. MZ and TX built the model and wrote the paper.

4 **Competing interests**.

5 The authors declare that they have no conflict of interest.

6 **Acknowledgements**: This work was supported by the National Key R&D Program of China

7 (2019YFC1407704), the National Nature Science Foundation of China (51879028), and the Open Fund of

8 State Key Laboratory of Coastal and Offshore Engineering, Dalian University of Technology (LP2009).

10 **References**

11 Alebregtse, N.C., and de Swart, H.E.: Effect of river discharge and geometry on tides and net water

12   transport in an estuarine network, an idealized model applied to the Yangtze Estuary. Cont. Shelf Res.,

13   123, 29-49, https://doi.org/10.1016/j.csr.2016.03.028, 2016.

14 Andrews, S.W, Gross, E.S., and Hutton, P.H.: Modeling salt intrusion in the San Francisco Estuary prior to

15   anthropogenic influence. Cont. Shelf Res., 146, 58-81, https://doi.org/10.1016/j.csr.2017.07.010, 2017.

16 Bowen, M.M., & Geyer, W.R.: Salt transport and the time-dependent salt balance of a partially stratified

17   estuary. J. Geophys. Res., 108(C5), 3158, https://doi.org/10.1029/2001JC001231, 2003.

18 Chen, C.S., Beardsley, R,C., Cowles, G.: An unstructured grid, finite-volume coastal ocean model FVCOM

19   user manual. SMAST/UMASSD, 2006.

20 Chen, C.S., Beardsley, R.C., and Cowles, G.: An unstructured grid, finite-volume coastal ocean model

21   (FVCOM) system. Oceanography, 19(1), 78-89, https://doi.org/10.5670/oceanog.2006.92, 2006.

22 Chen, C.S., Liu, H.D., and Beardsley, R.C.: An unstructured grid, finite-volume, three-dimensional,

primitive equations ocean model: application to coastal ocean and estuaries. J. Atmos. Ocean. Technol., 20 (1), 159-186, https://doi.org/10.1175/1520-0426, 2003.

Danish Hydraulic Institute (DHI): MIKE 21 Toolbox Global Tide Model—Tidal prediction. DHI Water and Environment, Hørsholm, Denmark, 2017.

Gong, W.P., Lin, Z.Y., Chen, Y.Z., Chen, Z.Y., and Zhang, H.: Effect of winds and waves on salt intrusion in the Pearl River estuary. Ocean Sci., 14, 139-159, https://doi.org/10.5194/os-14-139-2018, 2018.

Gong, W.P., and Shen, J.: The response of salt intrusion to changing river flow and tidal amplitude during winter season in the Modaomen Estuary, Pearl River Delta area, China. Cont. Shelf Res., 31(7-8), 769-788, https://doi.org/10.1016/j.csr.2011.01.011, 2011.

Gronewold, A.D., Anderson, E.J., and Smith, J.: Evaluating operational hydrodynamic models for real-time simulation of evaporation from large lakes. Geophys. Res. Lett., 46(6), 3263-3269, https://doi.org/10.1029/2019GL082289, 2019.

Haney, R.L.: On the Pressure Gradient Force over Steep Topography in Sigma Coordinate Ocean Models. J. Phys. Oceanogr. 21, 610–619, https://doi.org/10.1029/1999JC900188, 1990.

Hansen, D.V., and Rattray, M.: Gravitational circulation in straits and estuaries. J. Mar. Res., 23, 104-122, 1965.

Haralambidou, K., Sylaios, G., and Tsihrintzis, V.A.: Salt-wedge propagation in a Mediterranean micro-tidal river mouth. Estuar. Coast. Shelf S., 90(4), 174-184, https://doi.org/10.1016/j.ecss.2010.08.010, 2010.

Jia H., Shen, Y.M., Su, M.R., and Yu, C.X.: Numerical simulation of hydrodynamic and water quality effects of shoreline changes in Bohai Bay. Front. Earth Sci., 12(3), 625-639, https://doi.org/10.1007/s11707-018-0688-x, 2018.

Lai, W.F., Pan, J.Y., and Devlin, A.T.: Impact of tides and winds on estuarine circulation in the Pearl River Estuary. Cont. Shelf Res., 168(15), 68-82, https://doi.org/10.1016/j.csr.2018.09.004, 2018.

Lerczak, J.A., Geyer, W.R., and Chant, R.J.: Mechanisms driving the time-dependent salt flux in a partially stratified estuary. J. Phys. Oceanogr., 36(12), 2296-2311, https://doi.org/10.1175/JPO2959.1, 2006.

Li, S.H., Ge, Z.M., Xie, L.N., Chen, W., Yuan, L., Wang, D.Q., Li, X.Z., and Zhang, L.Q. Ecophysiological response of native and exotic salt marsh vegetation to waterlogging and salinity: Implications for the effects of sea-level rise. Sci. Rep., 8, 2441. https://doi.org/10.1038/s41598-017-18721-z, 2018.

Lin, Y.H., and Fissel, D.B.: High resolution 3-D finite-volume coastal ocean modeling in lower Campbell River and Discovery Passage, British Columbia, Canada. J. Mar. Sci. Eng., 2(1), 209-225, https://doi.org/10.3390/jmse2010209, 2014.

Liu, C.J., Yu, M.H., Jia, L.W., Cai, H.Y., and Chen, X.Q.: Impacts of physical alterations on salt transport during the dry season in the Modaomen Estuary, Pearl River Delta, China. Estuar. Coast. Shelf S., 227, 106345, https://doi.org/10.1016/j.ecss.2019.106345, 2019.

Liu, H., Yin, B.S., Xu, Y.Q., and Yang D.Z.: Numerical simulation of tides and tidal currents in Liaodong Bay with POM. Progress in Natural Science, 15(1): 47-55, https:// DOI: 10.1080/10020070512331341760, 2005

MacCready, P.: Calculating estuarine exchange flow using isohaline coordinates. J. Phys. Oceanogr., 41, 1116-1124, https://doi.org/10.1175/2011JPO4517.1, 2011.

McClain, M.E., Boyer, E.W., Dent, C.L., Gergel, S.E., Grimm, N.B., Groffman, P.M., Hart, S.C., Harvey, J.W., Johnston, C.A., Mayprga, E., McDowell, W.H., and Pinay, G.: Biogeochemical hot spots and hot moments at the interface of terrestrial and aquatic ecosystems. Ecosystems, 6(4), 301-312, https://doi.org/10.1007/s10021-003-0161-9, 2003.

1   Popescu, I., Cioaca, E., Pan, Q., Jonoski, A., and Hanganu, J.: Use of hydrodynamic models for the

2   management of the Danube Delta wetlands: The case study of Sontea-Fortuna ecosystem. Environ. Sci.

3   Policy, 46, 48-56, https://doi.org/10.1016/j.envsci.2014.01.012, 2015.

4   Pritchard, D.W.: Salinity distribution and circulation in the Chesapeake Bay estuaries system. J. Mar. Res.,

5   11, 106-123, 1952.

6   Pritchard, D.W.: A study of the salt balance in a coastal plain estuary. J. Mar. Res., 13, 133-144, 1954.

7   Qiao, H.T., Zhang, M.L., Jiang, H.Z., Xu, T.P., and Zhang, H.X.:. Numerical study of hydrodynamic and

8   salinity transport processes in the Pink Beach wetlands of the Liao River estuary, China. Ocean Sci., 14,

9   437-451, https://doi.org/10.5194/os-14-437-2018, 2018.

10   Ralston, D.K., Geyer, W.R., and Lerczak, J.A.: Subtidal salinity and velocity in the Hudson River estuary:

11   observations   and   modeling.   J.   Phys.   Oceanogr.,   38,   753-770,

12   https://doi.org/10.1175/2007JPO3808.1, 2008.

13   Sassi, M.G., and Hoitink, A.J.F.: River flow controls on tides and tide-mean water level profiles in a tidal

14   freshwater river. J. Geophys. Res., 118(9), 4139-4151, https://doi.org/10.1002/jgrc.20297, 2013.

15   Scully, M.E., and Geyer, W. R.: The role of advection, straining, and mixing on the tidal variability of

16   estuarine stratification. J. Phys. Oceanogr., 42(5):855-868, https://doi.org/10.1175/JPO-D-10-05010.1,

17   2012.

18   Song, J., Chen, M., Feng, G., Jia, Y.H., Wang, B.S., and Zhang, F.S.: Effect of salinity on growth, ion

19   accumulation and the roles of ions in osmotic adjustment of two populations of *Suaeda salsa*. Plant Soil,

20   314, 133-141, https://doi.org/10.1007/s11104-008-9712-3, 2009.

21   Sun, Z.G., Mou, X.J., and Sun, W.L.: Potential effects of tidal flat variations on decomposition and nutrient

22   dynamics of *Phragmites australis*, *Suaeda salsa*, and *Suaeda glauca* litter in newly created marshes of

the Yellow River Estuary, China. Ecol. Eng., 93, 175-186, https://doi.org/10.1016/j.ecoleng.2016.05.024, 2016.

Tian, R.: Factors controlling saltwater intrusion across multi-time scales in estuaries, Chester River, Chesapeake Bay. Estuar. Coast. Shelf S., 223, 61-73, https://doi.org/10.1016/j.ecss.2019.04.041, 2019.

Tsihrintzis, V.A., John, D.L., and Tremblay, P.J.: Hydrodynamic modeling of wetlands for flood detention. Water Resour. Manag., 12(4), 251-269, https://doi.org/10.1023/A:1008031011773, 1998.

Veerapaga, N., Azhikodan, G., Shintani, T., Iwamoto, N., and Yokoyama, K.: A three-dimensional environmental hydrodynamic model, Fantom-Refined: Validation and application for salt water intrusion in a meso-macrotidal estuary. Ocean Model., 141, 101425, https://doi.org/10.1016/j.ocemod.2019.101425, 2019.

Wang, J., Li, L., He, Z.G., Kalhoro, N.A., and Xu, D.F.: Numerical modelling study of seawater intrusion in Indus River Estuary, Pakistan. Ocean Eng., 184, 74-84, https://doi.org/10.1016/j.oceaneng.2019.05.029, 2019.

Wang, Y., Liu, R.H., Gao, H.W., Bai, J., and Ling, M.: Degeneration mechanism research of *Suaeda heteroptera* wetland of the Shuangtaizi Estuary National Nature Reserve in China. Procedia Enviro. Sci., 2, 1157-1162, https://doi.org/10.1016/j.proenv.2010.10.124, 2010.

Wang, Y.N., Sun, Z., Ji, Y.P., Zhang, M.L.: Analysis of *Suaeda heteroptera* cover change and its driving factors in the wetlands of the Liao River Estuary, China. IOP Conference Series: Earth and Environmental Science, 467, 2020.

Weilhoefer, C.L.: A review of indicators of estuarine tidal wetland condition. Ecol. Indic., 11, 514-525, https://doi.org/10.1016/j.ecolind.2010.07.007, 2011.

Yang, J.S., Zhan, C., Li, Y.Z., Zhou, D., Yu, Y., and Yu, J.B.: Effect of salinity on soil respiration in relation

1   to dissolved organic carbon and microbial characteristics of a wetland in the Liaohe River estuary,

2   Northeast China. Sci. Total Environ., 642, 946-953, https://doi.org/10.1016/j.scitotenv.2018.06.121,

3   2018.

4 Zhao, L.Z., Chen, C.S., Vallino, J., Hopkinson, C., Beardsley, R.C., Lin, H.C., and Lerczak, J.: Wetland-

5   estuarine-shelf interactions in the Plum Island Sound and Merrimack River in the Massachusetts coast.

6   J. Geophys. Res., 115(C10), 039, https://doi.org/10.1029/2009JC006085, 2010.